Intramolecular Hydrogen Bonding-Based Topology Regulation of Two-Dimensional Covalent Organic Frameworks

Intramolecular Hydrogen Bonding-Based Topology Regulation of Two-Dimensional Covalent Organic Frameworks

Yongwu Peng,§ Liuxiao Li,§ Chongzhi Zhu, Bo Chen, Meiting Zhao, Zhicheng Zhang, Zhuangchai Lai, Xiao Zhang, Chaoliang, Tan, Yu Han, Yihan Zhu* and Hua Zhang*

ABSTRACT: Creating molecular networks with different topologies using identical molecular linkers is fundamentally important, but requires a precise chemistry control. Here, we propose an effective strategy to regulate network topologies of two-dimensional (2D) covalent organic frameworks (COFs) through conformation switching of molecular linkages. By simply altering the substituents of an identical molecular linker, the topology-selective synthesis of two highly crystalline 2D COFs can be readily achieved. Their distinct crystal structures are observed and determined by low-dose high-resolution transmission electron microscopy imaging, indicating that the driving force for linkage conformation switching is intramolecular hydrogen bonding. Our strategy would greatly diversify the COF topologies and enable vast post-synthetic modifications like boron complexation, endowing these structures with unique optical property, such as fluorescence "turn on" and "aggregation-induced emission".

1. INTRODUCTION

Covalent organic frameworks (COFs), as one of emerging class of porous crystalline materials built from organic building blocks connected by covalent bonds,[1-9] have attracted widespread attention due to their various potential applications including gas adsorption and separation,[10-13] catalysis,[14-18] optoelectronics,[19-22] *etc.*[23-31] The functional diversity of COFs originates from their high structural tunability and versatility, in which a large variety of organic building blocks can be interconnected to create an almost infinite number of networks.[6-9] The overall properties of such porous materials are associated with their compositions and morphologies, but more critically rely on their network topologies.[32,33] Generally, the underlying topologies of two-dimensional (2D) COFs are greatly determined by the connectivity and symmetries of the building blocks involved. Once the symmetries of building blocks of a 2D COF are chosen, the regulation of substituents of building blocks has limited effects on the topologies of COF networks.[34-36] Recently, Pang *et al*. have demonstrated that the introduction of bulky alkyl substituents into an identical molecular linker could play a key role in switching the topology of a 2D COF due to the steric repulsion effect.[32] Unfortunately, the obtained product with uncommon topology exhibits poor crystallinity. Therefore, it is highly desired to design and synthesize topology-selective 2D COF networks with high crystallinity based on identical molecular linkers.

As known, it is quite challenging to directly identify and determine the topologies of COF networks. In most cases, COF topologies are modelled by the structural simulation, verified by the powder X-ray diffraction (PXRD) measurements combined with other physicochemical characterizations.[37,38] However, sometimes inconsistent results might be obtained.[39,40] The recent advance in the low-dose high-resolution transmission electron microscopy (HRTEM) has paved the way towards the direct imaging and structure determination of electron beam-sensitive materials at the atomic level.[41-43] Using this technique, not only the detailed framework information including the pore architectures and building blocks in 2D COFs,[28] but also the local structure features such as crystal surfaces and interfaces,[44,45] encapsulated guest molecules[46] and point- or extended-defects[47] in metal organic frameworks (MOFs) can be identified.

Here, we demonstrate that the introduction of molecular linkages with flexible conformation in 2D COFs can provide additional degrees of freedom for their topologies. Specifically, we have successfully synthesized two highly crystalline 2D COFs, namely TPE-COF-OH and TPE-COF-OMe, with different topologies and porosities by activation or passivation of intramolecular hydrogen bonding, which switches the conformation of molecular linkages in the networks, leading to the topology regulation of COF networks. Furthermore, the corresponding COF topologies are determined by low-dose HRTEM imaging, and further confirmed by the PXRD analyses combined with the structural simulations and the N_2 sorption measurements. In addition, the presence of (N, O)-bidentate Schiff base moieties in TPE-COF-OH allows post-synthetic modifications such as boron complexation, yielding TPE-COF-BF_2 as a COF derivative that exhibits exciting fluorescence "turn on" and "aggregation-induced emission" properties.

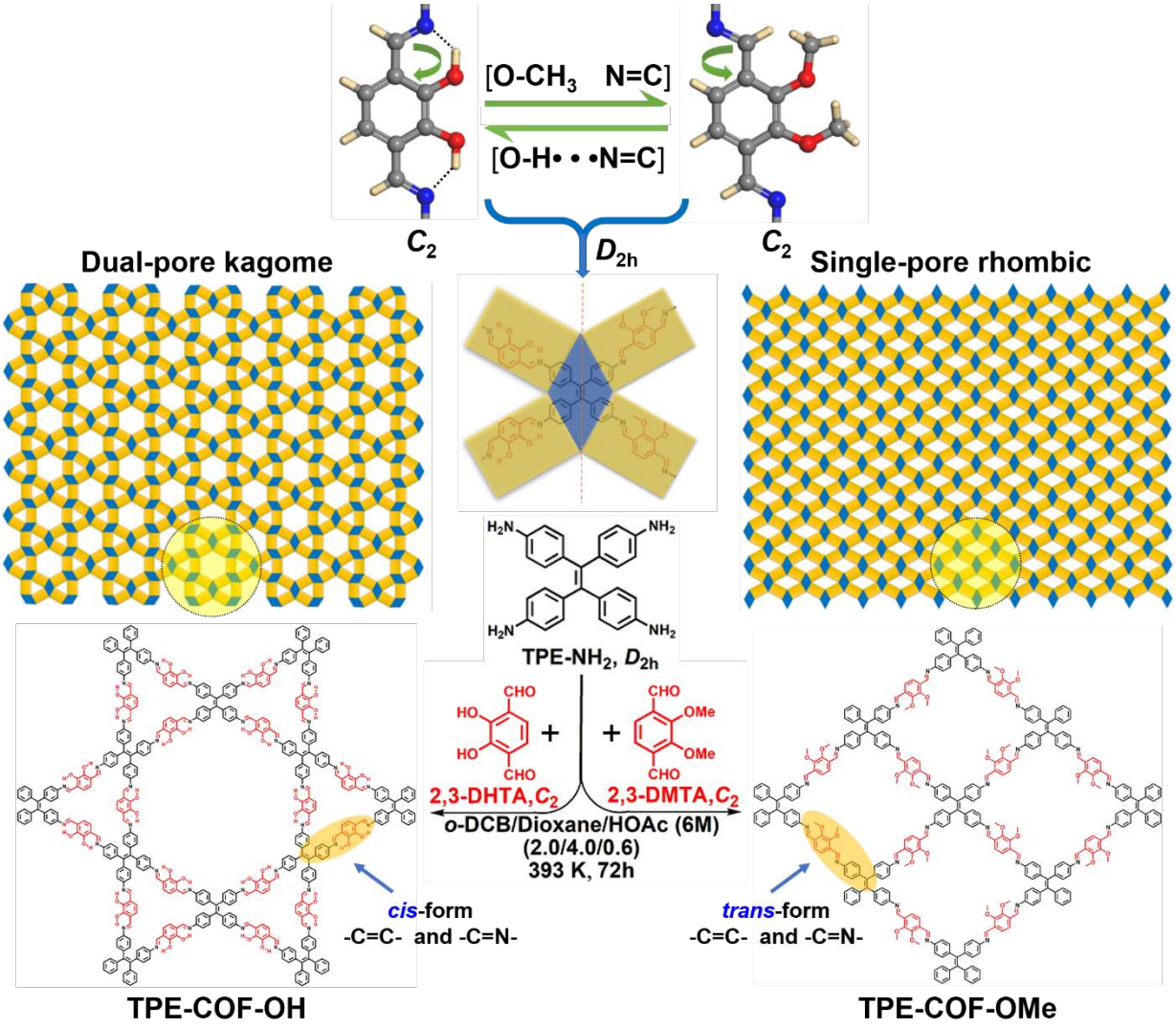

Scheme 1 Synthesis and topology diagrams of TPE-COF-OH and TPE-COF-OMe by the condensation of TPE-NH_2 with D_{2h} molecular symmetry and 2,3-DHTA/2,3-DMTA with C_2 molecular symmetry

2. RESULTS AND DISCUSSION

From the topological point of view, the combination of a 4-connected D_{2h}-symmetric building block with a 2-connected C_2-symmetric building block can theoretically lead to the formation of two different 2D COF networks, *i.e.*, a dual-pore kagome and a single-pore rhombic topology.[48] It provides an ideal model to investigate the effect of building blocks on the topology of 2D COFs. Since the conformation of molecular linkages in imine-linked 2D COF networks can be finely switched by virtue of intramolecular hydrogen bonding through tuning 2,3-substituted groups on terephthalaldehyde. In this work, the tetrakis(4-aminophenyl)ethane (TPE-NH_2) with D_{2h} molecular symmetry and 2,3-dihydroxyterephthalaldehyde (2,3-DHTA) or 2,3-dimethoxyterephthalaldehyde (2,3-DMTA) with C_2 molecular symmetry are chosen as building blocks to explore the effect of linkage conformation switching modulated by intramolecular hydrogen bonding in the topology regulation of 2D COFs. Specifically, through the Schiff base reaction between TPE-NH_2 and 2,3-DHTA (or 2,3-DMTA) in the mixture of *o*-dichlorobenzene (*o*-DCB)/dioxane/acetic acid (2:4:0.6, v:v:v) at 393 K for 72 h, TPE-COF-OH (or TPE-COF-OMe) was isolated as powder which cannot dissolve in common solvents (Scheme 1, see the detailed Experimental Section in the Supporting Information). The Fourier transform infrared (FT-IR) spectra of TPE-COF-OH and TPE-COF-OMe exhibit a characteristic C=N stretching band at 1619 cm^{-1}. Moreover, the aldehyde stretching bands of starting materials, *i.e.*, 1658 cm^{-1} for 2,3-DHTA and 1686 cm^{-1} for 2,3-DMTA, are greatly attenuated, indicating the condensation reaction happened and the formation of imine bonds (Figures S1-S2). Thermogravimetric analysis (TGA) analyses reveal that these two COFs show good thermal stability up to ca. 400 °C. The presence of a gradual weight loss for TPE-COF-OMe in the temperature range between 340 to 400 °C is attributed to the decomposition of methoxy groups in TPE-COF-OMe (Figure S3). As shown in the scanning electron microscopy (SEM) and transmission electron microscope (TEM) images, the morphologies of TPE-COF-OH and TPE-COF-OMe are hexagonal nanosheet and rectangular nanobelt, respectively (Figures S4a-b and S5a-b).

Recently, besides HRTEM imaging achieved on COFs,[49-51] low-dose HRTEM imaging integrated with direct detection electron-counting camera has been developed to provide structural solutions for a wide range of beam-sensitive materials,[41-43] like MOFs[44-47] and 2D COFs.[28] In this work, the 2D crystal structures of TPE-COF-OH and TPE-COF-OMe are imaged by

HRTEM using such a low-dose strategy (see the detailed Experimental Section in the Supporting Information). Electron diffraction patterns of these two 2D COFs along the [001] direction confirm a hexagonal symmetry for TPE-COF-OH and an orthorhombic symmetry for TPE-COF-OMe (Figure S6). In addition, the observed extinction rules of TPE-COF-OMe with h = 2n and k = 2n for (h00) and (0k0) reflections indicate the presence of 2_1 screw axes parallel to the *a* and *b* axes, respectively. As shown in Figure 1a, the HRTEM image and corresponding fast Fourier transform (FFT) pattern of TPE-COF-OH have been obtained along the [001] direction with a total electron dose of ~ $28e^{-}$ $Å^{-2}$. The hexagonally arranged star-shaped bright contrasts surrounded by dark contours are clearly observed in the chemically interpretable contrast transfer function (CTF)-corrected and denoised HRTEM image (Figure 1b). The contrast of the projected structure can be more clearly observed from a real-space motif-averaged image (Figure 1c). Based on these observations, the bright and dark contrasts can be assigned to the 1D open hexagonal/triangular channels and the COF network composed of the 4-connected TPE-NH_2 and 2-connected DHTA molecular fragments, respectively.

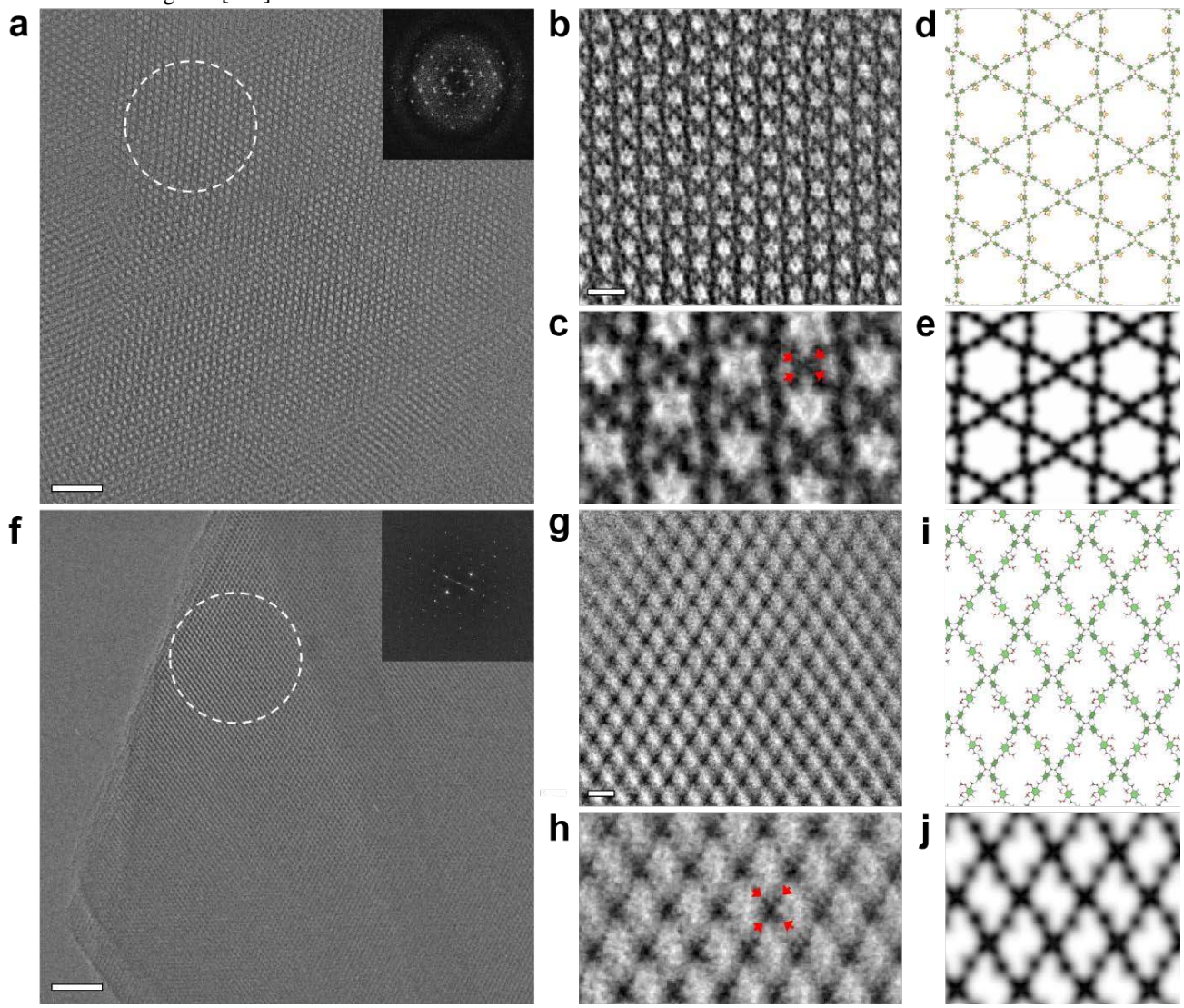

Figure 1 Low-dose HRTEM characterization of TPE-COF-OH and TPE-COF-OMe. (a) Low-dose motion-corrected HRTEM image of a representative TPE-COF-OH. Inset: FFT obtained from the white dashed circle. Scale bar: 20 nm. (b) CTF-corrected HRTEM image of the TPE-COF-OH based on a -200 nm defocus value, which is denoised by a Wiener filter. Scale bar: 5 nm. (c) Motif-averaged HRTEM image of the TPE-COF-OH. (d) Projected structural model and (e) simulated projected potential map of the TPE-COF-OH. A specific point-spread-function (PSF) width of 4.0 Å was used for TPE-COF-OH. (f) Low-dose motion-corrected HRTEM image of a representative TPE-COF-OMe. Inset: FFT obtained from the white dashed circle. Scale bar: 20 nm. (g) CTF-corrected HRTEM image of the TPE-COF-OMe based on a -426 nm defocus value, which is denoised by a Wiener filter. Scale bar: 5 nm. (h) Motif-averaged HRTEM image of the TPE-COF-OMe. (i) Projected structural model and (j) simulated projected potential map of the TPE-COF-OMe. A specific point-spread-function (PSF) width of 3.5 Å was used for TPE-COF-OMe.

These two different types of molecular fragments appear as dark dots and can be well distinguished from each other based on their distinct connectivity in the image. The TPE-NH_2 fragments can be identified by the characteristic "four claws" contrast associated with the four benzene rings (see the red arrows labeled in Figure 1c), while the connections between them are assigned to the DHTA fragments. It is worth mentioning that

the dark dot contrast for the DHTA fragment is much darker than expected, which can be attributed to the chemical bonding between Na^+ ions and the exposed hydroxy groups of the DHTA fragments,[52] verified by the energy-dispersive X-ray spectroscopy (EDS) analysis of the TPE-COF-OH (Figure S7). The positions of captured Na^+ ions identified from the contrast distortion towards the center of hexagonal channel can further help to determine the orientations of hydroxy groups in the network. Based on the aforementioned results, the crystal structure model for TPE-COF-OH with a *P*6 symmetry is proposed (Figure 1d and Tables S1-S2), and the simulated projected potential (Figure 1e) matches well with the CTF-corrected (Figure 1b) and motif-averaged image (Figure 1c).

Similarly, the TPE-COF-OMe can be imaged by HRTEM along the [001] direction with a total electron dose of ~ 20 e^- $Å^{-2}$ (Figure 1f). Based on the CTF-corrected and denoised image (Figure 1g) along with the motif-averaged image (Figure 1h), the crystal structure model for TPE-COF-OMe composed of identical molecular fragments with those in TPE-COF-OH can be proposed (Figure 1i and Tables S3-S4), based on their respective connectivity and "four claws" (see the red arrows labeled in Figure 1h) contrast. The image contrast matches well with the simulated projected potential (Figure 1j). The TPE-COF-OMe exhibits a rhombic-shape network different from the star-pore network in TPE-COF-OH. The positions of methoxy groups in TPE-COF-OMe structure are not directly observed in the HRTEM image, but can be determined based on the extinction rules and the $P2_12_12$ symmetry of the network.[47]

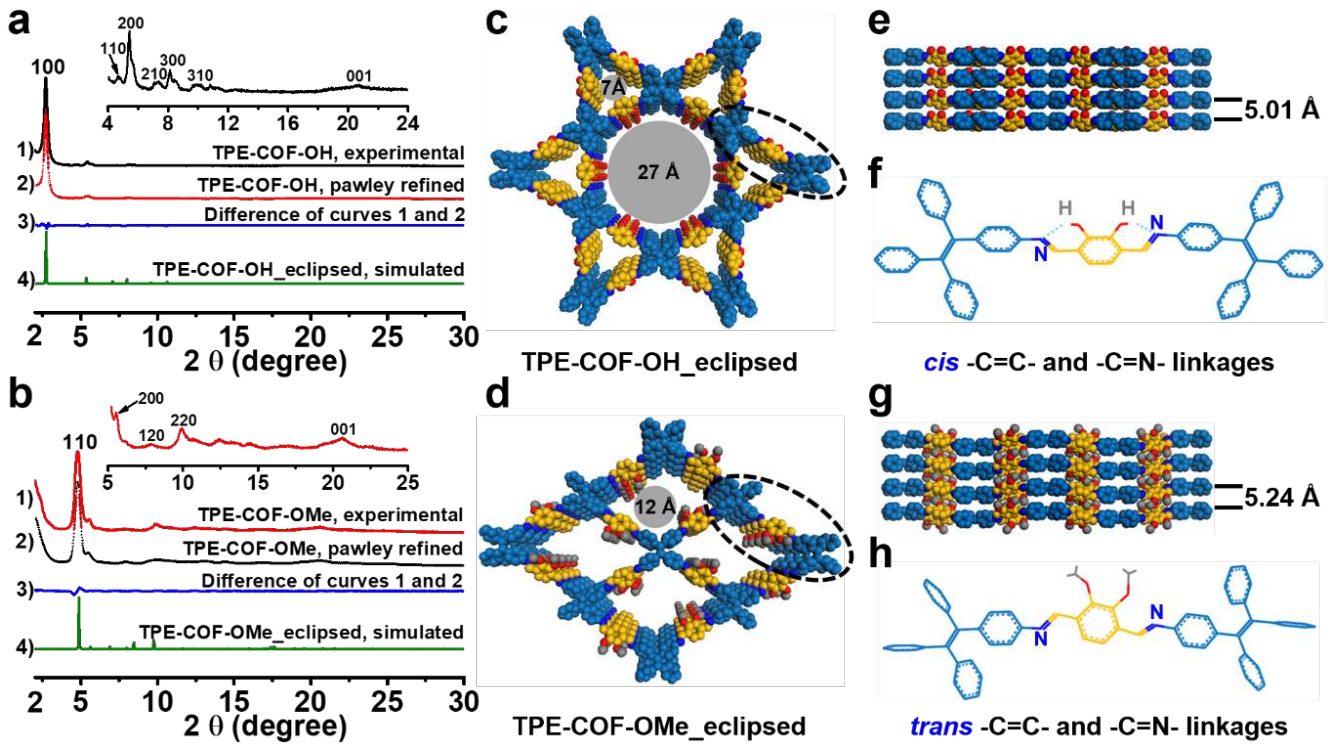

Figure 2 Characterization of TPE-COF-OH and TPE-COF-OMe. (a,b) Experimental and simulated PXRD patterns of TPE-COF-OH (a) and TPE-COF-OMe (b). Insets: high-magnification experimental PXRD patterns of TPE-COF-OH (a) and TPE-COF-OMe (b). (c,d) Crystal structures of TPE-COF-OH (c) and TPE-COF-OMe (d), assuming the eclipsed 2D stacking models of dual-pore kagome and single-pore rhombic topologies, respectively, viewed along the [001] direction. (e) Eclipsed stacking model of TPE-COF-OH viewed along the [100] direction with the interlayer distance of 5.01 Å. (f) Stick diagram of 2,3-DHTA molecular linker from the black dashed circle in (c), showing the presence of the intramolecular hydrogen bonding. All C=C and C=N linkages are in the *cis* conformation. (g) Eclipsed stacking model of TPE-COF-OMe viewed along the [100] direction with the interlayer distance of 5.24 Å. (h) Stick diagram of 2,3-DMTA molecular linker from the black dashed circle in (d). All C=C and C=N linkages are in the *trans* conformation.

The crystal structures and unit cell parameters of TPE-COF-OH and TPE-COF-OMe were further verified by the PXRD measurements combined with structural simulations (Figures 2a-b and Tables S1-S4). Base on low-dose HRTEM imaging in conjunction with the connectivity and geometries of the building blocks, two types of structural models with hexagonal *P*6 and orthorhombic $P2_12_12$ space groups were built accordingly.[53] The experimental PXRD pattern of TPE-COF-OH (curve 1 in Figure 2a) is in good agreement with the simulated PXRD pattern acquired using the 2D hexagonal eclipsed stacking model (curve 4 in Figure 2a). The PXRD profile of TPE-COF-OH shows a strong diffraction peak at 2.71° together with some weak peaks at 4.72°, 5.43°, 7.30°, 8.12° and 9.91°, which are assigned to the (100), (110), (200), (210), (300) and (310) reflection planes, respectively. The experimental PXRD pattern of TPE-COF-OMe (curve 1 in Figure 2b) exclusively reproduces the simulated PXRD pattern acquired using the 2D orthorhombic eclipsed stacking model (curve 4 in Figure 2b). The TPE-COF-OMe exhibits a main diffraction peak originating from the (110) reflection plane at 4.78°, as well as some weak peaks at 5.53°, 7.86° and 9.91°, corresponding to the (200), (120) and (220) reflection planes, respectively. The presence of broad (001) reflection planes at higher 2θ angles, *i.e.*, 20.69° in TPE-COF-OH (curve 1 in Figure 2a) and 20.59° in TPE-COF-OMe (curve 1 in Figure 2b), suggests the short coherence length

of 2D sheets along the c axis. To obtain a more accurate correlation with the experimental PXRD profile and elucidate the unit cell parameters, Pawley refinement was conducted. The Pawley-refined PXRD profiles of TPE-COF-OH (curve 2 in Figure 2a) and TPE-COF-OMe (curve 2 in Figure 2b) match well with their experimental PXRD profiles, indicated by their inappreciable difference (curve 3 in Figure 2a, and curve 3 in Figure 2b), with factors of R_{wp} and R_p converged to 3.82% and 5.72% for TPE-COF-OH, and 3.72% and 5.16% for TPE-COF-OMe. The Pawley refinement yielded the hexagonal unit cell with parameters of a = b = 38.7587 Å, c = 5.0105 Å for TPE-COF-OH, and the orthorhombic unit cell with parameters of a = 31.4076 Å, b = 22.1729 Å, and c = 5.2386 Å for TPE-COF-OMe. Such grid stacking along the c axis results in one-dimensional pore channels with pore sizes of ca. 7 Å and 27 Å in TPE-COF-OH (Figure 2c), and ca. 12 Å in TPE-COF-OMe (Figure 2d). The interlayer distances of TPE-COF-OH and TPE-COF-OMe were estimated to be 5.01 Å (Figure 2e) and 5.24 Å (Figure 2g), respectively. This difference in topologies of these two COFs can be ascribed to the activation and passivation of intramolecular hydrogen bonding in TPE-COF-OH and TPE-COF-OMe, respectively. In TPE-COF-OH, the existence of intramolecular hydrogen bonding interaction between the imine nitrogen and the hydroxy group of the aldehyde core ([O-H• • •N=C]) induces all imine and olefin bonds of TPE-COF-OH into the *cis* conformation, resulting in the hexagonal topology (Figure 2f). On the contrary, TPE-COF-OMe does not contain such hydrogen bonding interaction, as the TPE-NH_2 blocks are connected by 2,3-DMTA blocks in which the hydroxy groups in 2,3-DHTA are replaced by methoxy groups. As a result, all imine and olefin bonds of TPE-COF-OMe are in the *trans* conformation (Figure 2h), subsequently leading to the orthorhombic topology.

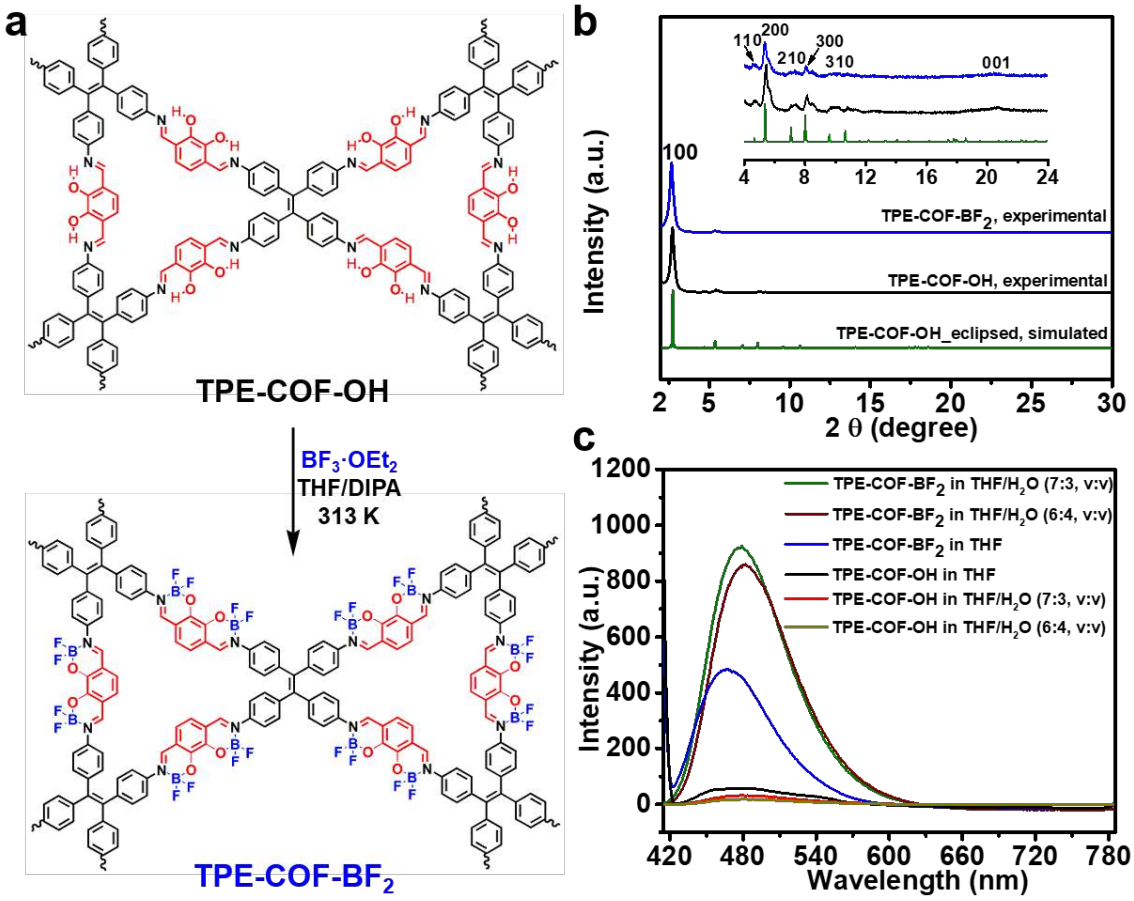

Figure 3 Synthesis and fluorescence study of TEP-COF-BF_2. (a) Schematic illustration of the synthesis of TPE-COF-BF_2 by the boron complexation of TPE-COF-OH. (b) Experimental and simulated PXRD patterns of TPE-COF-OH and TPE-COF-BF_2. Inset: high-magnification experimental and simulated PXRD patterns of TPE-COF-OH and TPE-COF-BF_2. (c) Fluorescence emission spectra of TPE-COF-OH and TPE-COF-BF_2 in the THF/H_2O mixed solution with water fraction from 0 to 40 vol%. Both the concentrations of TPE-COF-OH and TPE-COF-BF_2 are 12 μg mL^{-1}. The excitation wavelength is 400 nm.

The assigned topologies for TPE-COF-OH and TPE-COF-OMe were further verified by N_2 sorption isotherm measurements performed at 77 K (Figure S8). TPE-COF-OH features a characteristic type IV sorption isotherm with a step between P/P_0 = 0.10-0.20, indicative of its mesoporous character. In comparison, TPE-COF-OMe exhibits the reversible type I sorption isotherm, suggesting its microporous structure. The Brunauer-Emmett-Teller (BET) surface areas of TPE-COF-OH and TPE-COF-OMe were evaluated to be 1422 m^2 g^{-1} and 746 m^2 g^{-1}, respectively. Pore size distributions estimated based on nonlocal density functional theory (NLDFT) reveal two main pore distributions of ca. 7 Å and 25 Å for TPE-COF-OH and one narrow pore distribution of ca. 12 Å for TPE-COF-OMe, which are in good agreement with their predicted pore sizes according to their modelled structures (Figures 2c-d).

Owing to the strong π–π stacking interactions and rotationally variable imine linkages in 2D COFs, most of the imine-linked 2D COFs based on the previously reported TPE-NH_2

building blocks are non-fluorescent or weakly fluorescent.[48,54,55] In the study of imine-linked organic fluorophores, the covalent complexation of guest molecules with imine bonds has been demonstrated as an efficient strategy to restrict the rotation of imine bonds and subsequently suppress its effect in fluorescence quenching.[56,57] Considering the sheet-shaped morphology and the abundant existence of (N, O)-bidentate Schiff base moieties in TPE-COF-OH, the boron complexation of TPE-COF-OH and the fluorescence property were studied. As shown in Figure 3a, by reaction of the solvent-free TPE-COF-OH and the boron trifluoride etherate in the presence of N, N-diisopropylethylamine (DIPA) at 313 K for 12 h, the boron complexed TPE-COF-OH, namely TPE-COF-BF_2, was synthesized (see the detailed Experimental Section in the Supporting Information). Compared to the TPE-COF-OH, TPE-COF-BF_2 shows almost identical diffraction peaks (Figure 3b), indicating their isoreticular crystal structures. Moreover, the morphology of TPE-COF-OH is well preserved in TPE-COF-BF_2 (Figures S4a,c and S5a,c). The BET surface area and pore size of TPE-COF-BF_2 are determined to be 1188 $m^2 g^{-1}$ and ca. 23 Å, respectively, which are smaller compared to TPE-COF-OH (1422 $m^2 g^{-1}$ and ca. 25 Å) (Figure S8), suggesting the graft of BF_2 groups in TPE-COF-BF_2. The successful preparation of TPE-COF-BF_2 was further confirmed by TGA (Figure S3), FT-IR (Figure S9), and UV-Vis diffuse reflectance spectroscopy (Figure S10). As shown in Figure 3c, the fluorescence emission spectrum analysis reveals that TPE-COF-OH dispersed in THF at 25 °C only emits a very weak luminescence at 468 nm after excitation at 400 nm (black curve). After the boron complexation, the obtained TPE-COF-BF_2 displays a prominent enhancement of luminescence (blue curve), which is ca. 8 times that of TPE-COF-OH in intensity under the identical conditions. Interestingly, addition of a certain amount of water (ca. 30 vol%) in TPE-COF-BF_2 dispersed in THF causes a further enhancement of fluorescence intensity, indicating the typical aggregation-induced emission (AIE) characteristic of TPE-COF-BF_2 (olive curve). Upon further increasing the fraction of water (ca. 40 vol%), a slight decrease of fluorescence intensity was observed, which may be attributed to the precipitation of TPE-COF-BF_2 from solution (wine curve). The AIE behavior of TPE-COF-BF_2 is quite similar to that of boron complexed (N, O)-bidentate Schiff base organic fluorophores reported previously.[56] In contrast, TPE-COF-OH does not show the AIE behavior, evidenced by the gradual decrease of fluorescence intensity with the increased amount of water in THF (red curve for 30 vol% and dark yellow curve for 40 vol%). The enhanced fluorescence property of TPE-COF-BF_2 could be attributed to its increased rigidity and the resulting elimination of electron transfer from imine linkage to COF skeleton.

3. CONCLUSION

In summary, we have demonstrated that switching the linkage conformation in 2D COFs can effectively regulate their topologies. By simply altering the substituents of an identical molecular linker to introduce/eliminate intramolecular hydrogen bonding, two highly crystalline 2D COFs with different topologies and porosities have been synthesized, and their structures have been unraveled by low-dose HRTEM imaging combined with other characterizations. Furthermore, the (N, O)-bidentate Schiff base moieties in TPE-COF-OH can be used for boron complexation to generate unique optical properties, including fluorescence "turn on" and "aggregation-induced emission". Our unique strategy sheds light on the precise design and synthesis of 2D COFs with specific topology and unique property, which might be used for diverse promising applications.

ASSOCIATED CONTENT

Supporting Information.

The Supporting Information is available free of charge on the ACS Publications website. Experimental procedures and characterization data, including Figures S1-S10 and Table S1-S4.

AUTHOR INFORMATION

Corresponding Author

Hua Zhang - *Department of Chemistry, City University of Hong Kong, Hong Kong, China and Hong Kong Branch of National Precious Metals Material Engineering Research Center (NPMM), City University of Hong Kong, Hong Kong, China; orcid.org/0000-0001-9518-740X; Email: hua.zhang@cityu.edu.hk*

Yihan Zhu - *Center for Electron Microscopy, State Key Laboratory Breeding Base of Green Chemistry Synthesis Technology, College of Materials Science and Engineering and College of Chemical Engineering, Zhejiang University of Technology, Hangzhou, 310014, China; Email: yihanzhu@zjut.edu.cn*

Authors

Yongwu Peng - *Center for Programmable Materials, School of Materials Science and Engineering, Nanyang Technological University, 50 Nanyang Avenue, Singapore 639798, Singapore and Center for Electron Microscopy, State Key Laboratory Breeding Base of Green Chemistry Synthesis Technology, College of Materials Science and Engineering and College of Chemical Engineering, Zhejiang University of Technology, Hangzhou, 310014, China; orcid.org/0000-0003-4760-5173.*

Liuxiao Li - *Center for Programmable Materials, School of Materials Science and Engineering, Nanyang Technological University, 50 Nanyang Avenue, Singapore 639798, Singapore.*

Chongzhi Zhu - *Center for Electron Microscopy, State Key Laboratory Breeding Base of Green Chemistry Synthesis Technology, College of Materials Science and Engineering and College of Chemical Engineering, Zhejiang University of Technology, Hangzhou, 310014, China.*

Bo Chen - *Center for Programmable Materials, School of Materials Science and Engineering, Nanyang Technological University, 50 Nanyang Avenue, Singapore 639798, Singapore; orcid.org/0000-0001-6743-9251.*

Meiting Zhao - *Center for Programmable Materials, School of Materials Science and Engineering, Nanyang Technological University, 50 Nanyang Avenue, Singapore 639798, Singapore; orcid.org/0000-0002-0776-5626.*

Zhicheng Zhang - *Center for Programmable Materials, School of Materials Science and Engineering, Nanyang Technological University, 50 Nanyang Avenue, Singapore 639798, Singapore.*

Zhuangchai Lai - *Center for Programmable Materials, School of Materials Science and Engineering, Nanyang Technological University, 50 Nanyang Avenue, Singapore 639798, Singapore; orcid.org/0000-0001-8743-6568.*

Xiao Zhang - *Center for Programmable Materials, School of Materials Science and Engineering, Nanyang Technological University, 50 Nanyang Avenue, Singapore 639798, Singapore.*

Chaoliang Tan - *Department of Electrical Engineering, City University of Hong Kong, Hong Kong, China; orcid.org/0000-0003-1695-5285.*

Yu Han - *Physical Sciences and Engineering Division, Advanced Membranes and Porous Materials Center, King Abdullah University of Science and Technology (KAUST), Thuwal 23955-6900, Saudi Arabia; orcid.org/0000-0003-1462-1118.*

Author contributions

§ Y. W. Peng and L. X. Li contributed equally to this work.

Notes

The authors declare no competing financial interest.

ACKNOWLEDGMENT

This work was supported by MOE under AcRF Tier 2 (MOE2016-T2-2-103; MOE2017-T2-1-162) in Singapore. Y. Zhu acknowledges the financial support from the National Natural Science Foundation of China (Grant No. 21771161) and Thousand Talents Program for Distinguished Young Scholars. We would like to acknowledge the Facility for Analysis, Characterization, Testing and Simulation, Nanyang Technological University, Singapore, for use of their electron microscopy (and/or X-ray) facilities. H.Z. thanks the financial support from ITC via Hong Kong Branch of National Precious Metals Material Engineering Research Center (NPMM), and the start-up grant (Project No. 9380100) and grants (Project No. 9610478 and 1886921) in City University of Hong Kong.

REFERENCES

(1) Côté, A. P.; Benin, A. I.; Ockwig, N. W.; O'Keeffe, M.; Matzger, A. J.; Yaghi, O. M. Porous, crystalline, covalent organic frameworks. *Science* **2005**, *310*, 1166-1170.

(2) Ding, S. Y.; Wang, W. Covalent organic frameworks (COFs): from design to applications. *Chem. Soc. Rev*. **2013**, *42*, 548-568.

(3) Colson, J. W.; Dichtel, W. R. Rationally synthesized two-dimensional polymers. *Nat. Chem*. **2013**, *5*, 453-465.

(4) Diercks, C. S.; Yaghi, O. M. The atom, the molecule, and the covalent organic framework. *Science* **2017**, *355*, 923-930.

(5) Kandambeth, S.; Dey, K.; Banerjee, R. Covalent Organic Frameworks: Chemistry beyond the Structure. *J. Am. Chem. Soc*. **2019**, *141*, 1807-1822.

(6) Huang, N.; Wang, P.; Jiang, D. Covalent Organic Frameworks: A Materials Platform for Structural and Functional Designs. *Nat. Rev. Mater*. **2016**, *1*, 16068.

(7) Jin, Y.; Hu, Y.; Zhang, W. Tessellated Multiporous Two-Dimensional Covalent Organic Frameworks. *Nat. Rev. Chem*. **2017**, *1*, 0056.

(8) Chen, X.; Geng, K.; Liu, R.; Tan, K. T.; Gong, Y.; Li, Z.; Tao, S.; Jiang, Q.; Jiang, D. Covalent Organic Frameworks: Chemical Approaches to Designer Structures and Built-In Functions. *Angew. Chem., Int. Ed*. **2019**, *59*, 5050-5091.

(9) Geng, K.; He, T.; Liu, R.; Dalapati, S.; Tan, K.; Li, Z.; Tao, S.; Gong, Y.; Jiang, Q.; Jiang, D. Covalent Organic Frameworks: Design, Synthesis, and Functions. *Chem. Rev*. **2020**, Doi: 10.1021/acs.chemrev.9b00550.

(10) Furukawa, H.; Yaghi, O. M. Storage of Hydrogen, Methane, and Carbon Dioxide in Highly Porous Covalent Organic Frameworks for Clean Energy Applications. *J. Am. Chem. Soc*. **2009**, *131*, 8875-8883.

(11) Doonan, C. J.; Tranchemontagne, D. J.; Glover, T. G.; Hunt, J. R.; Yaghi, O. M. Exceptional Ammonia Uptake by a Covalent Organic Framework. *Nat. Chem*. **2010**, *2*, 235-238.

(12) Zeng, Y.; Zou, R.; Zhao, Y. Covalent Organic Frameworks for CO2 Capture. *Adv. Mater*. **2016**, *28*, 2855-2873.

(13) Wang, Z. F.; Zhang, S. N.; Chen, Y.; Zhang, Z. J.; Ma. S. Q. Covalent organic frameworks for separation applications, *Chem. Soc. Rev*. **2020**, *49*, 708-735.

(14) Ding, S. Y.; Gao, J.; Wang, Q.; Zhang, Y.; Song, W. G.; Su, C. Y.; Wang, W. Construction of Covalent Organic Framework for Catalysis: Pd/COF-LZU1 in Suzuki-Miyaura Coupling Reaction. *J. Am. Chem. Soc*. **2011**, *133*, 19816-19822.

(15) Stegbauer, L.; Schwinghammer, K.; Lotsch, B. V. A hydrazone-Based Covalent Organic Framework for Photocatalytic Hydrogen Production. *Chem. Sci*. **2014**, *5*, 2789-2793.

(16) Fang, Q.; Gu, S.; Zheng, J.; Zhuang, Z.; Qiu, S.; Yan, Y. 3D Microporous Base-Functionalized Covalent Organic Frameworks for Size-Selective Catalysis. *Angew. Chem., Int. Ed*. **2014**, *53*, 2878-2882.

(17) Lin, S.; Diercks, C. S.; Zhang, Y. B.; Kornienko, N.; Nichols, E. M.; Zhao, Y. B.; Paris, A. R.; Kim, D.; Yang, P.; Yaghi, O. M.; Chang, C. J. Covalent Organic Frameworks Comprising Cobalt Porphyrins for Catalytic CO2 Reduction in Water. *Science* **2015**, *349*, 1208-1213.

(18) Wang, X.; Han, X.; Zhang, J.; Wu, X.; Liu, Y.; Cui, Y. Homochiral 2D Porous Covalent Organic Frameworks for Heterogeneous Asymmetric Catalysis. *J. Am. Chem. Soc*. **2016**, *138*, 12332-12335.

(19) Wan, S.; Guo, J.; Kim, J.; Ihee, H.; Jiang, D. A Belt-Shaped, Blue Luminescent, and Semiconducting Covalent Organic Framework. *Angew. Chem., Int. Ed*. **2008**, *47*, 8826-8830.

(20) Bertrand, G. H.; Michaelis, V. K.; Ong, T. C.; Griffin, R. G.; Dincă, M. Thiophene-Based Covalent Organic Frameworks. *Proc. Natl. Acad. Sci. U. S. A*. **2013**, *110*, 4923-4928.

(21) Dogru, M.; Bein, T. On the Road Towards Electroactive Covalent Organic Frameworks. *Chem. Commun*. **2014**, *50*, 5531-5546.

(22) Calik, M.; Auras, F.; Salonen, L. M.; Bader, K.; Grill, I.; Handloser, M.; Medina, D. D.; Dogru, M.; Lobermann, F.; Trauner, D.; Hartschuh, A.; Bein, T. Extraction of Photogenerated Electrons and Holes from a Covalent Organic Framework Integrated Heterojunction. *J. Am. Chem. Soc*. **2014**, *136*, 17802-17807.

(23) Chandra, S.; Kundu, T.; Kandambeth, S.; BabaRao, R.; Marathe, Y.; Kunjir, S. M.; Banerjee, R. Phosphoric Acid Loaded Azo (-N=N-) Based Covalent Organic Framework for Proton Conduction. *J. Am. Chem. Soc*. **2014**, *136*, 6570-6573.

(24) Fang, Q.; Wang, J.; Gu, S.; Kaspar, R. B.; Zhuang, Z.; Zheng, J.; Guo, H.; Qiu, S.; Yan, Y. 3D Porous Crystalline Polyimide Covalent Organic Frameworks for Drug Delivery. *J. Am. Chem. Soc*. **2015**, *137*, 8352-8355.

(25) Lin, G.; Ding, H.; Yuan, D.; Wang, B.; Wang, C. A Pyrene-Based, Fluorescent Three-Dimensional Covalent Organic Framework. *J. Am. Chem. Soc*. **2016**, *138*, 3302-3305.

(26) Ding, S. Y.; Dong, M.; Wang, Y. W.; Chen, Y. T.; Wang, H. Z.; Su, C. Y.; Wang, W. Thioether-Based Fluorescent Covalent Organic Framework for Selective Detection and Facile Removal of Mercury(II). *J. Am. Chem. Soc*. **2016**, *138*, 3031-3037.

(27) Wang, S.; Wang, Q.; Shao, P.; Han, Y.; Gao, X.; Ma, L.; Yuan, S.; Ma, X.; Zhou, J.; Feng, X.; Wang, B. Exfoliation of Covalent Organic Frameworks into Few-Layer Redox-Active Nanosheets as Cathode Materials for Lithium-Ion Batteries. *J. Am. Chem. Soc*. **2017**, *139*, 4258-4261.

(28) Peng, Y. W.; Huang, Y.; Zhu, Y. H.; Chen, B.; Wang, L. Y.; Lai, Z. C.; Zhang, Z. C.; Zhao, M. T.; Tan, C. L.; Yang, N. L.; Shao, F. W.; Han, Y.; Zhang, H. Ultrathin Two-Dimensional Covalent Organic Framework Nanosheets: Preparation and Application in Highly Sensitive and Selective DNA Detection. *J. Am. Chem. Soc*. **2017**, *139*, 8698-8704.

(29) Zhang, L.; Wang, S.-B.; Zhou, Y.; Wang, C.; Zhang. X. Z.; Deng, H. X. Covalent Organic Frameworks as Favorable Constructs for Photodynamic Therapy. *Angew. Chem., Int. Ed*. **2019**, *58*, 14213-14218.

(30) Biswal, B. P.; Valligatla, S.; Wang, M. C.; Banerjee, T.; Saad, N. A.; Murali Krishna Mariserla, M. B.; Chandrasekhar, N.; Becker, D.; Addicoat, M.; Senkovska, I.; Berger, R.; Rao, D. N.; Kaskel, S.; Feng, X. L. Nonlinear Optical Switching in Regioregular Porphyrin Covalent Organic Frameworks. *Angew. Chem., Int. Ed*. **2019**, *58*, 6898-6900.

(31) Zeng, J. Y.; Wang, X. S.; Xie, B. R.; Li, M. J.; Zhang, X. Z. Covalent Organic Framework for Improving Near-Infrared Light Induced Fluorescence Imaging through Two-Photon Induction. *Angew. Chem., Int. Ed*. **2020**, 59, 10087-10094.

(32) Pang, Z. F.; Zhou, T. Y.; Liang, R. R.; Qi, Q. Y.; Zhao, X. Regulating the Topology of 2D Covalent Organic Frameworks by the Rational Introduction of Substituents. *Chem. Sci*. **2017**, *8*, 3866-3870.

(33) Meng, Y.; Luo, Y.; Shi, J. L.; Ding, H. M.; Lang, X. J.; Chen, W.; Zheng, A. M.; Sun. J. L.; Wang. C. 2D and 3D Porphyrinic Covalent Organic Frameworks: The Influence of Dimensionality on Functionality. *Angew. Chem., Int. Ed*. **2019**, *58*, 16217-16222.

(34) Tilford, R. W.; Mugavero III, S. J.; Pellechia, P. J.; Lavigne, J. J. Tailoring Microporosity in Covalent Organic Frameworks. *Adv. Mater*. **2008**, *20*, 2741-2746.

(35) Zhang, J.; Han, X.; Wu, X.; Liu, Y.; Cui, Y. Multivariate Chiral Covalent Organic Frameworks with Controlled Crystallinity and Stability for Asymmetric Catalysis. *J. Am. Chem. Soc*. **2017**, *139*, 8277-8285.

(36) Wang, L. K.; Zhou, J. J.; Lan, Y. B.; Ding, S. Y.; Yu, W.; Wang, W. Divergent Synthesis of Chiral Covalent Organic Frameworks. *Angew. Chem., Int. Ed*. **2019**, *58*, 9443-9447.

(37) Ma, T.; Kapustin, E. A.; Yin, S. X.; Liang, L.; Zhou, Z.; Niu, J.; Li, L.; Wang, Y.; Su, J.; Li, J.; Wang, X.; Wang, W. D.; Wang, W.; Sun, J.; Yaghi, O. M. Single-Crystal X-ray Diffraction Structures of Covalent Organic Frameworks. *Science* **2018**, *361*, 48-52.

(38) Evans, A. M.; Parent, L. R.; Flanders, N. C.; Bisbey, R. P.; Vitaku, E.; Kirschner, M. S.; Schaller, R. D.; Chen, L. X.; Gianneschi, N. C.; Dichtel, W. R. Seeded Growth of Single-Crystal Two-Dimensional Covalent Organic Frameworks. *Science* **2018**, *361*, 52-57.

(39) Lan, Y.; Han, X.; Tong, M.; Huang, H.; Yang, Q.; Liu, D.; Zhao, X.; Zhong, C. Materials Genomics Methods for High-throughput Construction of COFs and Targeted Synthesis. *Nat. Commun*. **2018**, *9*, 5274.

(40) Zhang, B.; Mao, H. Y.; Matheu, R.; Reimer, J. A.; Alshmimri, S. A.; Alshihri, S.; Yaghi, O. M. Reticular Synthesis of Multinary Covalent Organic Frameworks. *J. Am. Chem. Soc*. **2019**, *141*, 11420-11424.

(41) Zhang, D. L.; Zhu, Y. H.; Liu, L. M.; Ying, X. R.; Hsiung, C. E.; Sougrat, R.; Li, K.; Han, Y. Atomic-resolution transmission electron microscopy of electron beam-sensitive crystalline materials. *Science* **2018**, *359*, 675-679.

(42) Song, K. P.; Liu, L. M.; Zhang, D. L.; Hautzinger, M. P.; Jin, S.; Han, Y. Atomic-Resolution Imaging of Halide Perovskites Using Electron Microscopy. *Adv. Energy Mater*. **2020**, 1904006.

(43) Chen, X. L.; Dwyer, C.; Sheng, G.; Zhu, C. Z.; Li, X. N.; Zheng, C. L; Zhu, Y. H. Imaging Beam-Sensitive Materials by Electron Microscopy. *Adv. Mater*. **2020**, *32*, 1907619.

(44) Zhu, Y. H.; Ciston, J.; Zheng, B.; Miao, X. H.; Czarnik, C.; Pan, Y. C.; Sougrat, R.; Lai, Z. P.; Hsiung, C. E.; Yao, K. X.; Pinnau, I.; Pan, M.; Han, Y. Unravelling surface and interfacial structures of a metal-organic framework by transmission electron microscopy. *Nat. Mater*. **2017**, *16*, 532-536.

(45) Li, X. H.; Wang, J. J.; Liu, X.; Liu, L. M.; Cha, D.; Zheng, X. L.; Yousef, A. A.; Song, K. P.; Zhu, Y. H.; Zhang, D. L.; Han, Y. Direct Imaging of Tunable Crystal Surface Structures of MOF MIL-101 Using High-Resolution Electron Microscopy. *J. Am. Chem. Soc*. **2019**, *141*, 12021-12028.

(46) Aulakh, D.; Liu, L. M.; Varghese, J. R.; Xie, H. M.; Islamoglu, T.; Duell, K.; Kung, C. W.; Hsiung, C. E.; Zhang, Y. X.; Drout, R. J.; Farha, O. K.; Dunbar, K. R.; Han, Y.; Wriedt, M. Direct imaging of isolated single-molecule magnets in metal-organic frameworks. *J. Am. Chem. Soc*. **2019**, *141*, 2997-3005.

(47) Liu, L. M.; Chen, Z. J.; Wang, J. J.; Zhang, D. L.; Zhu, Y. H.; Ling, S. L.; Huang, K. W.; Belmabkhout, Y.; Adil, K.; Zhang, Y. X.; Slater, B.; Eddaoudi, M.; Han, Y. Imaging defects and their evolution in a metal-organic framework at sub-unit-cell resolution. *Nat. Chem*. **2019**, *11*, 622-628.

(48) Zhou, T. Y.; Xu, S. Q.; Wen, Q.; Pang, Z. F.; Zhao, X. One-Step Construction of Two Different Kinds of Pores in a 2D Covalent Organic Framework. *J. Am. Chem. Soc*. **2014**, *136*, 15885-15888.

(49) Banerjee, T.; Haase, F.; Trenker, S.; Biswal, B. P.; Savasci, G.; Duppel, V.; Moudrakovski, I.; Ochsenfeld, C.; Lotsch, B. V. Sub-stoichiometric 2D covalent organic frameworks from tri- and tetratopic linkers. *Nat. Commun*. **2019**, *10*, 2689.

(50) Liang, R.; Xu, S.; Zhang, L.; A, R.; Cui, F.; Qi, Q.; Sun, J. L.; Zhao, X. Rational design of crystalline two-dimensional frameworks with highly complicated topological structures. *Nat. Commun*. **2019**, *10*, 4609.

(51) Sahabudeen, H.; Qi, H.; Ballabio, M.; Položij, M.; Olthof, S.; Shivhare, R.; Jing, Y.; Park, S. W.; Liu, K.; Zhang, T.; Ma, J.; Rellinghaus, B.; Mannsfeld, S.; Heine, T.; Bonn, M.; Cánovas, E.; Zheng, Z.; Kaiser, U.; Dong, R.; Feng. X. L. Highly Crystalline and Semiconducting Imine-Based Two-Dimensional Polymers Enabled by Interfacial Synthesis. *Angew. Chem., Int. Ed*. **2020**, *59*, 6028–6036.

(52) Weston, M. H.; Farha, O. K.; Hauser, B. G.; Hupp, J. T.; Nguyen, S. T. *Chem. Mater*. **2012**, *24*, 1292-1296.

(53) *Accelrys Materials Studio Release Note*s, 5.5, Accelrys Software, Inc., San Diego, **2010**.

(54) Ascherl, L.; Sick, T.; Margraf, J. T.; Lapidus, S. H.; Calik, M.; Hettstedt, C.; Karaghiosoff, K.; Döblinger, M.; Clark, T.; Chapman, K. W.; Auras, F.; Bein, T. Molecular docking sites designed for the generation of highly crystalline covalent organic frameworks. *Nat. Chem*. **2016**, *8*, 310-316.

(55) Auras, F.; Ascherl, L.; Hakimioun, A. H.; Margraf, J. T.; Hanusch, F. C.; Reuter, S.; Bessinger, D.; Doblinger, M.; Hettstedt, C.; Karaghiosoff, K.; Herbert, S.; Knochel, P.; Clark, T.; Bein, T. Synchronized Offset Stacking: A Concept for Growing Large-Domain and Highly Crystalline 2D Covalent Organic Frameworks. *J. Am. Chem. Soc*. **2016**, *138*, 16703-16710.

(56) Frath, D.; Benelhadj, K.; Munch, M.; Massue, J.; Ulrich, G. Polyanils and Polyboranils: Synthesis, Optical Properties, and Aggregation-Induced Emission. *J. Org. Chem*. **2016**, *81*, 9658-9668.

(57) Urban, M.; Durka, K.; Jankowski, P.; Serwatowski, J.; Luliński, S. Highly Fluorescent Red-Light Emitting Bis(boranils) Based on Naphthalene Backbone. *J. Org. Chem*. **2017**, *82*, 8234-8241.

Table of Contents artwork